Conf-920804--25

WSRC-MS--91-416

DE93 000593

DOWNWARD FLOW OF WATER WITH ENTRAINED AIR IN A NONUNIFORMALY HEATED SUBDIVIDED ANNULUS (U)

by

B. S. Johnston and C. P. May

Westinghouse Savannah River Company
Savannah River Site
Aiken, South Carolina 29808

A paper proposed for presentation at the
1992 ASME/AIChE NATIONAL HEAT TRANSFER CONFERENCE
San Diego, California
August 1992

and for publication in the proceedings

DISCLAIMER

Downward Flow of Water with Entrained Air in a Nonuniformly Heated Subdivided Annulus

B. S. Johnston and C. P. May
Westinghouse Savannah River Company
Aiken, South Carolina

ABSTRACT

This paper describes an experimental study in which water was fed to a vertical annulus, entraining air in downward flow. The annulus was subdivided by longitudinal fins into four subchannels and was heated with an azimuthally varying heat flux. A bypass was provided to simulate flow in parallel channels. For steady liquid flow, inlet temperature, and pressure boundary conditions, the power was increased until critical heat flux was reached. Overheating characteristics were grouped according to the prevailing flow pattern. In annular flows ($j_L < 0.3$ m/s) overheating of the whole test section occurs when steam production causes countercurrent flooding. In intermittent flows ($0.3 < j_L < 0.9$ m/s) the overheating is confined to a portion of the hot subchannel. The mechanism is postulated to be stagnation of a large bubble. In bubble flows (0.9 m/s $< j_L$) overheating occurs by diverting inlet flow to the bypass and again involves the whole test section. Except at the very lowest flow rates, critical heat flux occurs when the effluent liquid temperature is below saturation.

Unstable operation of parallel heated channels carrying a two-phase flow is usually discussed in terms of either the Ledinegg flow excursion or an oscillatory instability (Boure et al, 1973). In the former, a heated channel may enter a regime of two-phase flow in which the resistance to flow increases as the flow decreases. Flow is consequently diverted to the other channels, and the starved channel may overheat. Oscillatory instabilities are associated with fluctuation of the vapor content, flow, pressure, and so forth among the various channels. This may lead to overheating, as well.

This paper is also concerned with unstable operation and overheating in parallel channels. The channels of interest, however, are necessarily vertical and are fed water by gravity in such a way that air is entrained in a two-component, two-phase downward flow. The flow discharges from the heated channels at the bottom of a pool of liquid. Such a situation obtains in supplying emergency core coolant during a major loss-of-coolant accident (LOCA) in some types of nuclear reactor.

In Savannah River Site reactors, the reactor fuel is contained in several nested concentric tubes, which are separated by longitudinal fins and placed in an outer housing tube. The reactor core comprises some number of these nested assemblies, which are contained in a tank and cooled by downward flow from an upper plenum. At late stages of the hypothetical LOCA, the coolant is expected to form a pool in the upper plenum and flow by gravity through perforations in the outer housing of each assembly. It would then fall within the housing as a heavy rain until it reached the top of the fuel tubes. Here it would be distributed among the parallel annular channels, where it would entrain air. The air/water mixture would leave the bottom of each assembly into a common pool in the reactor tank.

The coolant must remove decay heat generated by the the fuel after the safety rods have been inserted into the core. Core cooling thus depends on the distribution of flow from the upper plenum pool into parallel assemblies, as well as the distribution of the falling flow into nested channels within each assembly. Should the coolant be prevented from entering at the top of any annular channel, there exist alternate paths for it. Consequently, flow instabilities which interrupt the delivery of coolant to a given channel will lead directly to overheating. Hence it is hypothesized that reactor damage can be avoided by preventing flow disturbances in the most limiting single channel.

The problem is then to examine a single heated annulus, fed by gravity with an available bypass for flow. The outer tube of the annulus is heated; the heat flux varies azimuthally to simulate unbalanced neutron flux in the reactor. The liquid flow rate and the pressure boundary conditions are imposed on the heater. Consistent with the context of parallel channels, the air flow rate is not set, but is rather a dependent variable. The power is increased until the outer tube overheats. Such information may be used to set appropriate limits on pre-accident reactor power.

BACKGROUND

Flow patterns for downward two-phase flow have been described by a number of investigators [Golan and Stenning,1969, Oshinowo and Charles, 1974, Yamazaki and Yamaguchi,1979, Spedding and Nguyen, 1980, Barnea et al, 1982, Crawford et al, 1985]. These studies have primarily featured air and water at atmospheric pressure, although Oshinowo and Charles [1974] used water-glycerol solutions and Crawford et al. [1985] used refrigerant and its vapor. There is, of course, some variation in the naming of flow patterns and the degree of discrimination invoked in description. Similarly, the investigators disagree on the conditions for transition between patterns, and how these are most effectively presented. However, the main features may be described by designating three primary patterns of flow: annular, intermittent, and bubble.

The annular flow pattern includes not only the sheared liquid film pattern which is familiar by this name in upward flow, but also a falling film condition, as well. Thus it exists at low liquid flow rates, whether gas flow is high or low. In either case, the void fraction is high. The bubble flow pattern generally occurs at high liquid flow rates. Neither Yamazaki and Yamaguchi [1979] nor Spedding and Nguyen [1980] observed bubble flow. In the former case, this may have been because the test section discharged into a gas space; in the latter case, relatively low superficial liquid velocities were used.

The intermittent pattern between these extremes is less easily characterized, with various investigators identifying slug, plug, froth, churn, intermittent, pulsating, or oscillatory patterns. Although Golan and Stenning [1969] include the slug pattern with bubble flow, the other investigators relate it more closely to the other intermittent patterns. While slug (or plug) and churn flows are reasonably distinct from one another in upward flow (see for example, McQuillan and Whalley [1985]), this appears less the case for downward flow.

The studies cited above have all concerned tubes. There appears to be no data available for downward flow in annuli, and certainly not subdivided annuli in particular. However, Kelessidis and Dukler [1989] identified the same four basic flow patterns for upward flow in an annulus that McQuillan and Whalley [1985],

among many others, did for upward flow in a tube. Hence, there is reasonable expectation that downward flow in an annulus might show similarities to those tube patterns discussed above.

Downward flow has been recognized as a cooling mechanism for vertical channels with bottom blockage. Block and Wallis [1978] describe how overheating, or critical heat flux (CHF), in such a channel may be related to flooding, or countercurrent flow limitation. Saturated liquid flows into the channel and is vaporized in its downward passage. Vapor flows upward; the highest countercurrent flows are found at the inlet. To determine the heat flux at the point of flooding, heat and mass balances on the channel are combined with the well-known flooding correlation of Wallis [1969] to obtain

$$\phi = \frac{C^2 h_{lg} A_f D_h^{1/2} [g \rho_g (\rho_l - \rho_g)]^{1/2}}{A_h [1 + (\rho_g/\rho_l)^{1/4}]^2} \tag{1}$$

where the empirical constant C is between 0.7 and 1.0. For a heat flux in excess of this, the vapor produced cannot admit the necessary liquid. Flooding thus reduces the liquid supply and the channel overheats. Because the mechanism depends on flow limitation and not local heat removal, it is the total heat duty of the channel and not the actual distribution of heat flux which determines the limiting criterion. For subcooled fluid inlet, the authors made an empirical correction to the latent heat of vaporization and obtained

$$\phi = \frac{C^2 \left(h_{lg} + 0.1 \left(\frac{\rho_l}{\rho_g} \right)^{3/4} C_p (T_s - T_i) \right) A_f D_h^{1/2} [g \rho_g (\rho_l - \rho_g)]^{1/2}}{A_h [1 + (\rho_g/\rho_l)^{1/4}]^2} \tag{2}$$

The heated channel is characterized in Equations (1) or (2) by its flow area, heated area, and a characteristic length D_h. Block and Wallis [1978] noted that several alternatives to the conventional hydraulic diameter have been used. Osakabe and Kawasaki [1989] proposed that data for flooding in the top of a rectangular passage is best correlated in terms of the span of the rectangle instead of its hydraulic diameter. This implies that the presence of fins in the rectangle can reduce the liquid flow rate by reducing the effective span. Their data for an annulus implied that the annulus

is effectively divided anyway, so that actual fins in the annulus may not influence the liquid delivery.

For a channel not closed at the bottom, countercurrent flow limitation may only apply at the lowest flow rates. Mishima and Nishihara (1985) heated a downward flow of water in a 2.4 by 40 mm rectangular test section. At the lowest flows, the vapor would rise against the liquid flow. Overheating indeed occurred near the entrance of the test section by countercurrent flow limitation; Equation (1) provided a good lower bound to the data. At larger flows, the bubbles were suspended in the test section, and overheating occurred over large areas. For these conditions, and greater than 35°C inlet subcooling, the outlet liquid was also subcooled. At yet higher flows, overheating was due to dry patches forming in a churn or annular flow. It was noted that the liquid tended to flow near the unheated narrow sides of the channel.

Mishima and Nishikawa compared a test section heated from both sides to another heated from only one. For a given mass flux, overheating in the two-sided channel occurred at about half the heat flux as it did in the one-sided test section. Thus they inferred that overheating was not dependent on the distribution of heat flux, but rather on the total power delivered to the test section.

Sudo et al. (1985) obtained CHF data for downward flow in a rectangular test section. To correlate their data, they invoked the notion of flooding, Equation (1), with the assumption that the liquid would be completely vaporized. This may be written

$$\phi = \frac{A_f}{A_h} G C_p (T_s - T_i) + \frac{C^2 h_{lg} A_f D_h^{1/2} [g \rho_g (\rho_l - \rho_g)]^{1/2}}{A_h [1 + (\rho_g/\rho_l)^{1/4}]^2} \qquad (3)$$

which is Equation (1) added to a sensible heat balance. The authors noted an oscillatory regime of downward flow, at unspecified liquid flow rate, in which vapor moved alternately with and against the downward liquid. In subsequent work, Sudo and Kaminaga (1989) determined a new flooding correlation for a rectangular channel and used this with their earlier CHF data to derive a new CHF correlation.

Guerrero (1990) studied CHF for downward flow with entrained air in a uniformly heated annulus. His apparatus featured a stainless steel heater and insulating fins attached to an unheated inner tube. CHF was signaled by either a temperature excursion or reverse flow of liquid into the air inlet lines. This latter condition was observed at the lowest and highest flow rates. By contrast, at intermediate flows only localized overheating was observed. Guerrero suggested that the condition of overheating depended on the total power supplied to the test section instead of the local heat flux. For all but the lowest flows, CHF occurred at subcooled outlet conditions.

The CHF studies of Mishima and Nishihara (1985) and Sudo et al. (1985) indicate that overheating may be expected at subcooled outlet for at least part of the flow range. Further, they indicate that it is the total power which is important to determining the CHF, and not the local details of the heat flux. This is consistent with observations by Guerrero (1990) in two-component flow. For flow in gravity-fed parallel channels particular attention needs to be paid to events which might lead to diversion of flow. Guerrero in particular discussed how inlet flow was disturbed at the inlet to the heated section.

EQUIPMENT AND OPERATION

Figure 1 is a schematic of the piping and loop instrumentation. Deionized water was circulated from a centrifugal pump through a strainer and flowmeter to the water distributor, shown in Figure 2. Here the water and entrained air flowed down into the annular test section. Air was fed to the distributor through a water-filled pressure regulator, which could be arranged for positive or negative inlet pressure.

The test section effluent flowed into four separator tubes for air disengagement, and then to an adjustable standpipe. The water returned to a mixing tank and then through a heat exchanger to the pump. The mixing tank served to damp out short term fluctuations in flow and temperature. Also, by using a recycle stream from the pump discharge, the temperature of the test section effluent was lowered to avoid flashing in either the pump or the heat exchanger.

Since the apparatus was intended to represent a heater in parallel with others, a test section bypass was provided. This comprised four pipe nipples pointing up at the

inlet to the heater, connected through vertical pipes to the base of the separator tubes. In normal operation, there was no flow in the bypass, as verified by observing the transparent sections in the pipes.

The test section comprised an outer heater tube and a finned, adiabatic inner piece. The fins separated the annulus into four subchannels, designated A through D. The overall test section dimensions are given in Table 1. The equivalent diameter was calculated considering the entire wetted surface and flow area, including that in the narrow gap between fins and outer wall.

Table 1.
Test Section Dimensions

Inner housing OD	68.2 mm
Rib circle diameter	75.3 mm
Heater ID	76.2 mm
Heater tube OD (before flame-spray)	82.7 mm
Rib width	3.2 mm
Cross-sectional area (incl fin clearance)	863 mm^2
Hydraulic diameter (incl all surfaces of fins)	7.2 mm

The heater was made by a flame-spray process. An aluminum base tube was rotated on a lathe bed, while a flame-spray jet traversed its length. The tube was first flame-sprayed with a 0.08 mm thick layer of nickel/aluminum composite. This served as a bonding layer for a subsequent 0.25 mm layer of aluminum oxide/titanium oxide. Following this, a layer of aluminum, nominally 0.15 mm thick, was applied. The aluminum layer actually varied in thickness with azimuthal position; this was done by making a regular variation in the rotation speed of the tube. It was this final aluminum layer which served as the heater, insulated from the rest of the apparatus by the underlying 0.7 Mohm ceramic layer. The heat flux distribution per subchannel, as percent of average heat flux, was A: 110%, B: 98%, C: 90%, D: 102%.

Loop instrumentation included liquid turbine flowmeters, a thermal air flow meter, and thermocouples for the inlet air, inlet water, and the effluent water. Voltage was measured across the heater and calibrated shunts in the DC power supply circuit. Pressure taps were spaced at 0.6 m along the test section. At each axial station there was one tap per subchannel. These were joined by a common impulse line to a pressure gauge. Deionized water was used to purge the lines prior to reading.

Sheathed thermocouples were pressed against the heater wall for 24 mm, parallel to the axis of the tube, before being led radially away. These thermocouples were supported on a ring attached locally to the heater, and thus able to move with the heater as it expanded. Other sheathed thermocouples protruded from the inner housing and bent upward 12 mm into the fluid space, midway between the walls. The heater and fluid thermocouples were arranged at 0.3 m spacing over the heated length. Most of these axial stations featured one thermocouple in the center of each subchannel. Two stations, however, featured three fluid and heater thermocouples per subchannel, spaced at 22.5°; an additional four heater thermocouples were deployed over the fins.

The data acquisition system comprised two microcomputers, each scanning 80 A/D channels at 1 Hz. At each scan of the channels, calibration constants were applied to the flowmeters, pressure gauges, and voltage measurements to produce quantities in engineering units for display and storage. Scanning was done continuously for monitoring; logging of data was done on demand. In a log file, each scan had a date and time-of-day stamp; in addition, each scan read a millisecond timer to document any variations and skips in the scan record.

In normal operation, the rig was run at a series of steady states until a condition was found at which the tube overheated. A given inlet pressure and standpipe level, as well as inlet temperature, were set. The liquid was circulated at a given flow rate. The power was increased, usually in 2 to 3 kW increments, and the equipment allowed to run for 10 minutes. At the end of this period, the instruments might be logged, and the power was increased again. In the event of any wall temperature rising to 250°C, the power was shut off as the instruments were logged. New flow, temperature, and pressure conditions were set, and this process was repeated. All data reported in this paper were taken with inlet at 45°C and atmospheric pressure, and the outlet standpipe at 0, 0.9, or 1.8 m.

Thermocouples were checked against flowing isothermal water and condensing atmospheric steam and found to read within ±2°C of standard. The inlet temperature measurement was separately corrected to ±0.5°C uncertainty. Pressure gauges were good to ±0.3 kPa, flowmeters to ±1% of scale, and power measurements

to ±1 kW. The uncertainty in calculated results is estimated by conventional sum-of-squares combination.

UNHEATED FLOW

Data for unheated flow are used to determine flow patterns. These are then shown to exhibit distinctive characteristics in normal heated operation, as well as the process of overheating.

Visual Identification of Flow Patterns in a Transparent Test Section.

Liquid/gas flow patterns were observed in a demonstration rig comprising a finned tube forming a subdivided annulus in an outer transparent tube. Like the heated apparatus described above, this transparent rig was arranged to draw in air from the atmosphere and discharge into a pool of liquid. These observations apply to the flow of liquid with entrained air between fixed pressure boundary conditions. A comprehensive description for all combinations of liquid and gas flow rates is not intended.

With no flow, the bottom of the test section is filled with water at the level of the discharge pool. As liquid is supplied at low rates, the water flows in a film down the walls and fins of the annulus. Increasing the flow rate causes the film to develop surface waves and entrain some bubbles into the standing liquid, but no net gas is carried through. The test section thus exhibits two distinct regions. Both liquid and gas are continuous in the upper part of the test section; liquid is continuous in the lower. This is termed the annular flow pattern.

At higher flow rates, the liquid is observed to bridge the channel gap and thus break up the continuous column of gas. In addition, the liquid velocity is sufficient to carry bubbles through the column of liquid to the outlet. Thus net entrainment of gas begins. With further flow increase, the occlusions begin to take the form of long bubbles. In analogy with flow in circular conduits, these will be called Taylor bubbles. The rounded nose is upward, against the flow; the lower end is ragged. The Taylor bubbles are confined to individual subchannels, with occasional leakage across a fin clearance. They are alternately broken up and then increased by agglomeration to lengths about ten times the circumferential distance between fins. They alternately rise against the flow and are swept downward. Because of the

strong axial mixing, this is termed the intermittent flow pattern. In general, the flow has lost its two-region character; the bottom of the test section appears to be little different from the top.

With further increase in liquid flow, the Taylor bubbles become shorter. They tend to be largest in the middle of the test section, and break up in the bottom. The gas is dispersed in the liquid as small spherical bubbles, with occasional cap-shaped bubbles. The vigorous axial mixing of the intermittent flow pattern is not so pronounced. This is the bubble flow pattern. Further increases in the liquid flow rate would ultimately force the apparatus to fill up. Air entrainment would cease as the liquid flooded the inlet flow distributor. At this point the pressure gradient would be that for single phase flow in the test section.

Pressure Profiles and Air Entrainment

In the heated apparatus, there is no visual access. Hence, the flow patterns described above must be inferred from flow and pressure measurements. The transition between intermittent and bubble flow is indicated by two considerations. First, the frictional pressure drop is estimated. The mixture momentum balance for one dimensional downward adiabatic flow relates the static pressure gradient to its frictional and gravitational components.

$$-\frac{dP}{dz} = -\left[\frac{dP}{dz}\right]_f - g[\langle\alpha\rangle\rho_g + (1-\langle\alpha\rangle)\rho_l] \tag{4}$$

The cross-sectional average void fraction in the gravitational term is assumed to be described by the drift flux model of Zuber and Findlay [1965].

$$\frac{\langle j_g\rangle}{\langle\alpha\rangle} = C_o\langle j\rangle + \langle\langle V_{gj}\rangle\rangle \tag{5}$$

Clark and Flemmer [1984] found Equation (5) to describe their data for downward air/water flow in a pipe. In the absence of information specific to a finned annulus, the distribution coefficient is assumed to be 1.2 and the weighted mean drift velocity to be -0.25 m/s. These values were intermediate in the ranges quoted by Clark and Flemmer, representing their data and that of others. The drift velocity is negative because it opposes the downward flow.

The void fraction model and experimental measurements of static pressure allow the frictional pressure drop to be found from Equation (4). This is expressed as a liquid pressure drop multiplier plotted versus the Martinelli parameter (see, e.g., Butterworth and Hewitt [1977]) in Figure 3. The data for three sets of standpipe liquid level tend to a common asymptote as liquid flow rate increases. This asymptote is taken to be representative of a fully-developed flow regime. Each data set reaches the asymptote at a liquid superficial velocity between 0.9 and 1.0 m/s.

Further information is derived from considering the fluctuating nature of the intermittent flow pattern. Because of the strong axial mixing, there is considerable time-variation in the rate of gas entrainment and movement through the test section. In Figure 4 is shown the standard deviation of the measured gas flow versus the imposed liquid superficial velocity. After a domain of fluctuating air flow, the fluctuations fall to a minimum at about 1 m/s, regardless of standpipe liquid level. This smoothing of the gas flow rate is indicative of the smaller bubbles and uniform downward motion in bubble flow. It occurs at about the same liquid superficial velocity which marks the asymptotic behavior of the pressure drop in Figure 3. These two characteristics are taken to define the intermittent-to-bubble flow pattern transition at a liquid superficial velocity of 0.9 to 1.0 m/s.

Figure 4 also shows the initiation of the fluctuations to begin between 0.2 and 0.3 m/s. Since the onset of intermittent flow is associated with the initiation of air entrainment, this should mark the transition from annular to intermittent flow. Further support for this is obtained by solving Equation (5) for the liquid superficial velocity at which the gas superficial velocity $\langle j_g \rangle$ is just zero.

$$\langle j_l \rangle = - \frac{\langle\langle V_{gj} \rangle\rangle}{C_o} \tag{6}$$

Equation (6) represents the liquid flow necessary to begin downward entrainment of gas bubbles in the liquid column at the bottom of the test section. From the drift flux parameter values specified above, $\langle j_l \rangle$ is found to be 0.2 m/s.

Figure 5 shows how the axial pressure profile varies with imposed liquid flow for a test with a 1.8 m standpipe level. In each profile, the inner four points represent the

test section itself. Note the positive pressure gradients in these gravity-fed flows. The profile at 0.29 m/s liquid superficial velocity is characterized by a two-region distribution, corresponding to a continuous gas column above a liquid column. This is characteristic of the annular flow pattern. On transition to intermittent flow, the gas phase is no longer continuous. The pressure profile at 0.44 m/s thus becomes almost linear. Further increases in liquid rate result in a lesser slope, indicating an increase in the frictional loss component. Other than differences in slope, there is little in the pressure profile to distinguish intermittent from bubble flow.

Figure 6 presents gas versus liquid superficial velocities at three different standpipe levels. Increasing the standpipe level, which steepens the positive pressure gradient, suppresses the flow of air. The annular-to-intermittent flow pattern transition criterion marks the onset of air entrainment for the cases with an exit liquid level. With no liquid in the standpipe, by contrast, it is not necessary to entrain gas bubbles through a liquid column. Hence, air entrainment begins at the lowest liquid flow. The points which are connected represent conditions on the friction loss asymptote in Figure 3. It may be noted that the transition to bubble flow portends a decline in gas flow rate.

The proposed flow pattern transition criteria are simple and provide a serviceable representation of various observations in unheated flow. They are intended to help organize the heated flow data to be presented below. Certainly refinements could be made, but this is neither possible, without more direct information on the void fraction, nor justified for the intended use.

HEATED FLOW

In this section are described the characteristics of heated operation at non-boiling conditions. The entrained air produces marked differences from single phase convective heat transfer. In particular, there is considerable transient behavior within an overall steady operation.

Time-Averaged Temperature

Due to the azimuthal variation in heat flux, the four subchannels differ in power input. If the fins provided a tight seal between them, the axial distribution of liquid

temperature for single phase liquid flow would take the form of four straight lines diverging from a common inlet temperature. These lines would be arranged about the equilibrium temperature calculated from the total power. As it happens, there is some mixing of liquid between subchannels. This reduces the spread between the temperature profiles and introduces some slight non-linearity, especially since the fin clearance is likely to vary in an undetermined manner with axial position. However, the profiles still cluster about the equilibrium temperature.

In two-phase flow, there are further divergences based on the distribution of phases and the possibility of axial mixing. Figure 7 shows time-averaged temperature profiles for an intermittent flow pattern. These are highly non-linear and, excepting subchannel C, lie above the expected equilibrium value. At the inlet of the test section, subchannels A and D heat up rapidly, while C runs cool. After about 1 m, these trends are arrested, as if some liquid has left subchannel C for the others. Subchannel A actually becomes cooler with increasing axial position. Guerrero [1990] noted that a contrived liquid distribution would change with axial position in his finned test section.

In a highly voided flow, like annular or intermittent, the air and vapor tend to flow near the subchannel center, while much of the subcooled liquid stays near the fins. This means that the temperature indicated by a fluid thermocouple does not represent the bulk averaged, or mixing-cup temperature. Rather, it is more indicative of the vapor temperature tempered by occasional passage of cooler liquid. Hence the fluid temperatures in Figure 7 must be understood not to represent the subchannel average.

Time-averaged temperature profiles for annular flows resemble those in Figure 7, with a significant difference. While the subchannel profiles will lie above equilibrium for most of the test section, they return to cluster around the equilibrium temperature for those fluid thermocouples immersed in the liquid column at the bottom. These, then, actually provide bulk temperature readings. On the other hand, bubble flow profiles resemble those for single-phase flow. The dispersion of air and vapor into small bubbles allows a thermocouple to spend a greater fraction of its time in the liquid, and hence, the near-single phase behavior.

In addition to this transverse phase distribution effect, temperature profiles are also influenced by axial distribution of the phases. The intermittent flow pattern features significant axial mixing. The rise of Taylor bubbles can transport vapor upstream to thermocouples in what would be expected to be a cooler region. Direct evidence for axial mixing comes from fluid thermocouples which are placed in the channel upstream of the start of heating. In Figure 7, subchannel A is significantly above the fluid inlet temperature at the left of the plot. This behavior is not observed in bubble flows, nor, curiously, in annular flows.

Figure 8 shows the azimuthal distribution of time-averaged wall and fluid temperature. Note that the temperatures are high in subchannel A and low in C. In addition, there is no particular effect associated with the fins. Although the actual geometry (that is, whether the fins are in contact) is not known at the thermocouple locations, it seems that no portion of the heated wall is blocked from effective heat transfer by the presence of the fin.

Fluctuating Temperatures

In heating single phase liquid flow, the time trace of a typical thermocouple placed in the fluid stream will feature a standard deviation of about 0.2°C. By contrast, if air is admitted to the flow at the same power, the measurement standard deviation may rise by a factor of 25 or so. Electrical noise and variation in the supplied power affect the two traces equally, and the liquid flow rate and inlet temperature are well controlled. This fluctuation in fluid temperature instead depends on the temporal and spatial distribution of the two phases under heating.

As an indicator of fluctuation level, the standard deviation was calculated for each of the 68 fluid thermocouples at a given power and flow rate. These were then averaged to produce a measure of variance for the entire test section at the prevailing conditions. Figure 9 is a plot of this averaged standard deviation versus power. The power has been normalized by the power required for saturated outlet temperature at the prevailing flow. The annular and bubble flow patterns are remarkably convergent, considering that the actual power levels vary significantly between them, and that the flow patterns are quite different. The intermittent flow pattern is distinctive in showing a much higher degree of temperature fluctuation.

This results to some extent from the axial mixing, as discussed above, and transient overheating, which will be discussed below.

Air Entrainment and Pressure Profiles

Figure 10 shows how air entrainment varies with increasing power at a given liquid flow rate. For intermittent and bubble flow patterns, the air intake drops off with increasing power. To a first approximation, this can be represented by assuming the void fraction to be determined solely by the liquid flow. By Equation (5) then, the gas phase flow should remain constant with increasing power. Water vapor makes up an increasing proportion of the gas phase, and less air is required. Representing the air/vapor mixture as an ideal gas, the results are shown on the figure. The trend is correct, but does not agree in detail with the data. To improve the description would require more detailed flow pattern modeling, incorporating appropriate interfacial stresses.

For annular flow, by contrast, the air rate suddenly rises when the outlet temperature nears saturation. As was shown in Figure 6, annular flow entrains little air when it is cold. However, the vapor produced as the power rises must be accomodated. In the other flow patterns, it has been suggested, vapor replaces air in the gas phase. In the annular flow pattern, the vapor may actually force a transition to intermittent flow. Evidence for this is given by the axial pressure profiles shown in Figure 11. Here the flow of liquid has not changed, but the two-region profile of the cold condition changes to indicate holdup of liquid in the test section. This occurs at about 90% of saturation, the point at which air entrainment begins, as shown in Figure 10. Furthermore, the fluid temperatures at this condition are at saturation over the lower two-thirds of the test section.

OVERHEATING

In boiling systems, the critical heat flux (CHF) represents a marked reduction in the ability of a flow to transfer heat from a solid surface. The result of this, for nuclear or electric heating, is a sharp increase in the temperature of the heater. In the present experiment, this took the form of a temperature excursion in response to an increase in applied power. A temperature excursion was declared when any wall temperature exceeded 250°C. The CHF was then defined as the mean of that heat flux which resulted in a temperature excursion and the previous lower

measurement. The resolution of this value was typically ±2.3 kW/m^2 at any flow rate. The various observations at the occurrence of CHF are collectively termed overheating.

The somewhat arbitrary 250°C wall temperature limit assumes that (1) without interrupting power, the test section would be damaged, or (2) the actual power necessary to cause this damage is negligibly larger than that necessary to set the wall at 250°C. In fact, plots of maximum measured wall temperature versus applied power do feature a steep gradient in the vicinity of the arbitrary 250°C criterion. Other temperature criteria would have given the same result, within the scatter of measurement.

Figure 12 presents the overheating power as a function of supplied liquid flow rate. Most of the data were obtained by increasing power, as described above. However, some were determined by holding power steady and decreasing flow in steps. In the figure, the power has been normalized by the power required for saturated outlet temperature. This leads to a pronounced minimum in the curves. Note that this normalization may be thought of as a measure of the efficiency of use of the coolant. Thus, the lowest flows are used the most efficiently, the mid-range are used the least efficiently, and the highest flows are intermediate. The efficiency of coolant use is one of several characteristics of the overheating which vary in a regular way with flow rate. In what follows, these observations will be related to the prevailing flow patterns.

The results are shown in Figure 12 for three different standpipe liquid levels. Increasing the liquid level in the standpipe is seen to reduce the efficiency of coolant use at a given flow rate. From Figure 6, the effect of increasing the standpipe level is to reduce the capacity of the liquid flow to entrain gas. According to the discussion concerning Figure 10, this implies reducing the capacity of the flow to remove vapor from the test section. The inability to remove vapor would be related to the stagnation of flow, cessation of cooling, and the onset of overheating.

Annular Flow

As indicated by the low flows in Figure 12, the annular flow pattern allows the test section effluent to reach saturation before overheating occurs. Saturation

temperatures are measured in all subchannels for some distance upstream of the exit. Naturally, subchannel A reaches this condition upstream of the others. At CHF, the tube temperature is high over a significant fraction of the length; all subchannels are generally affected. The fluid thermocouples read saturation temperature throughout the entire test section. Pressure profiles reach a maximum in the middle. The temperature excursion is accompanied by a heavy flow of liquid through the bypass lines.

Figure 13 shows wall temperatures averaged over five seconds just as power was shut off. Subchannel A is the hottest, but in all subchannels a temperature excursion is well underway. At powers just below the condition illustrated in Figure 13, the wall temperature in subchannel A was observed to rise significantly above its normal reading for periods of five to 20 seconds. With no variation in fluid temperature to cause the fluctuation, this indicates transitory dry conditions. These fluctuations were observed at 2.6 m, just above the standpipe level. By contrast, the overheating is focused upstream of this at 1.8 m, while the tube outlet is the coolest portion.

Guerrero [1990], Mishima and Nishihara [1985], and Sudo et al. [1985] suggested that low flow CHF could be explained by a flooding mechanism. The subcooled equation of Block and Wallis [1978] may be applied, as may the model of Sudo et al., following the recommendation of Osakabe and Kawasaki [1989] that the subchannel span be used as the characteristic length. Equations (2) and (3) are written in terms of the normalized power and plotted in Figure 14. Equation (3) does not consider subcooled boiling, and thus predicts only saturated outlet temperatures. Equation (2) can describe CHF at subcooled outlet conditions, but overpredicts at low flow rates.

In spite of the general unsatisfactory fit of these particular models to the data, the countercurrent flow limitation is thought to provide a valid CHF mechanism. Note that a conventional CHF experiment will feature overheating at the exit of a heated section. In this test, by contrast, the overheating occurs in the middle rather than at bottom. This indicates that upward flow of vapor diverts the inlet liquid, and is consistent with the observed flow in the bypass lines. The remaining liquid in the test section falls to the bottom or boils away, and the middle region overheats. The

axial position of overheating varies somewhat from test to test, but tends to be near the middle of the tube.

By contrast, the bottom of the tube remains relatively cool. Presumably, this occurs because the liquid level in the standpipe keeps this portion of the test section under water. It was noted from Figures 10 and 11 that the structure of an annular flow changes near saturation. However, this apparently prevents neither flow reversal in the upper test section nor effective cooling in the lower.

Bubble Flow

In bubble flow, CHF occurs with subcooled outlet, as shown at the high flows in Figure 12. At the power setting just below the onset of overheating, the fluid temperature profiles are generally straight and close to the equilibrium temperature. The wall temperatures are correspondingly well-behaved. On increasing the power, the overheating is violent. The wall temperatures undergo a rapid rise, usually in all subchannels. There is heavy liquid flow in the bypass lines and significant amounts of water blown out of the air/water separators at the test section outlet. There were instances of water being driven into the air inlet line, closing the air supply check valve. Pressures during the excursion are highest in the middle of the test section, and indeed the vapor and liquid are forced out both ends.

Guerrero [1990] suggested that excursions in his low void regime were the result of excursive, or Ledinegg instability. This corresponds to the bubble flow pattern of the present study. The trigger for instability is the production of significant vapor in the test section, causing an increase in the resistance to flow. Inlet water backs up in the distributor to overcome this resistance and is diverted into the bypass lines. With inlet flow reduced, the rate of vapor production quickly rises and results in the overheating phenomena described above.

In one-component boiling flows, the correlation of Saha and Zuber [1974] is often used to predict the point of net vapor generation.

$$\frac{\phi}{GC_p(T_s - T_b)} = 0.0065 \qquad Pe > 70{,}000 \tag{7}$$

If it may be presumed that net vapor generation corresponds to an increase in flow resistance, Equation (7) may be used as a lower limit for the onset of intrachannel flow excursion. Combining Equation (7) with a sensible heat balance for the present apparatus, the normalized power for net vapor generation is plotted in Figure 14. Just as the characteristics of the bubble flow pattern approach those of single phase flow, it can be seen that the CHF data approach this one-component boiling limit as an asymptote.

Once again in contrast to conventional CHF behavior, it is observed that the axial position of bubble flow overheating varies, but tends to be in the middle of the test section. This is hypothesized to be the result of the tendency of the boiling flow to exit both ends of the test section after the inlet has been diverted to the bypass. The top and bottom are cooled by the escaping two-phase flow; the middle, having supplied the flow, is left to overheat. However, this is not always the case. Overheating has occasionally occurred at the bottom of the test section, and in one instance, the highest temperatures actually occurred at the very inlet.

Intermittent Flow

In intermittent flow, the least efficient use is made of coolant, as indicated by the minima in Figure 12. As power is increased, subchannel A will exhibit significant rises in wall temperature; the high temperature may persist from 5 to 30 seconds, and then decreases. CHF, in marked contrast to the other flow patterns, involves no diversion of flow through the bypass lines. Furthermore, the overheating in intermittent flow involves only about one-fourth the length of the hottest subchannel, occasionally with portions of another. Time-averaged wall temperature profiles for intermittent flow, in contrast to those in Figure 13, will show subchannel A overheated and the other subchannels in their normal state.

The CHF is less clearcut in intermittent flow than in the other flow patterns. Instead of temperature excursions marked by bypass flow and heating of the whole test section, the intermittent pattern required that the 250°C temperature criterion be invoked. The characteristic fluctuations often left the operator poised to shut off power while a temperature trace meandered along just under 250°C, finally to cool off without his intervention. Furthermore, overheating was not always observed immediately on increasing power. There were instances of the temperature

criterion being reached nearly seven minutes after the power had been increased. This variability in the behavior may account for some degree of scatter among repeated tests.

The proposed mechanism for this mode of overheating is local dryout under a stagnant bubble in a single subchannel. Visual observations indicated that Taylor bubbles could move up or down and were a frequent feature of intermittent flow. In a ten minute period, there are quite a number of bubbles formed. Only a small fraction of these would need to satisfy the right balance of forces to remain motionless while the wall film dried out. The supply of vapor within a bubble tends to maintain it against the disruptive forces of the downward flowing liquid.

This mechanism would explain the localized nature of the overheating and the lack of disturbance to the overall flow. It would also explain the transient heating and spontaneous cooling which is peculiar to the intermittent flow regime. This behavior is a great contributor to the overall level of fluctuation of temperature which was illustrated above in Figure 9. The annular and bubble flow patterns have no similar mechanism for producing variation in temperature.

Earlier, Equation (6) was used to estimate the onset of gas entrainment at a liquid superficial velocity 0.2 m/s. Also using drift flux arguments, Mishima and Nishihara [1985] calculated a liquid superficial velocity of 0.17 m/s to stagnate flow in their rectangular test section. Clift et al. [1978] correlate the terminal velocity of a large bubble in a rectangular channel by

$$\frac{U_t}{\sqrt{g D_1}} \sqrt{\frac{\rho_l}{(\rho_l - \rho_g)}} = 0.23 + \frac{0.13 D_2}{D_1} \qquad (8)$$

where $D_2 < D_1$. Using the channel gap and the distance between fins as the smaller and larger dimensions respectively, the rise velocity for a subchannel is computed to be 0.17 m/s. These results indicate that Taylor bubbles would be swept out of rectangular channels at much lower liquid superficial velocities than those characteristic of the intermittent flow pattern. If the stagnant bubble dryout mechanism is correct in the present application, the bubble must be causing the diversion of liquid flow to other subchannels. Thus the formation of a local dry spot would be affected by the behavior of the entire test section.

Data at near 1.8 m standpipe level were culled from Guerrero [1990] for comparison in Figure 14 with 1.8 m standpipe data from the present study. In the range of intermittent flow, the data from the present study fall under those of Guerrero by about 10%. Assuming the mechanism of stagnant bubble dryout, the CHF should depend on the local heat flux. Hence, the present test section would behave no differently were the whole heater at a heat flux corresponding to that of the hot subchannel. If the normalized power is calculated on this basis, the intermittent regime data come into agreement with those of Guerrero, which were determined in a uniformly heated annulus.

This comparison provides only indirect support for the proposed mechanism, and several questions remain. It is not clear why the overheating should occur in the mid-region of the test section rather than at the exit, where the liquid is presumably hotter. Furthermore, the minima in the data of Figure 12 might imply a competion of influences whose effects vary with the overall liquid flow rate. Quantitative predictions and proof of this mechanism must await further study of the details of the intermittent flow pattern.

DISCUSSION

Figure 14 shows data from Mishima and Nishihara [1985] and Sudo et al. [1985], plotted without regard for the variations in inlet temperature and test section dimensions. The Mishima data were run at lower liquid superficial velocities than those used in the present study. Both subcooled and saturated outlet conditions are observed. The Sudo data extend to higher flow rates and are in general agreement with present observations.

The data of Guerrero [1990] are most directly comparable in apparatus and manner of operation. The relationship of CHF to local heat flux has been discussed above for the intermittent flow pattern. In annular flow, the data are not available at comparable standpipe levels to allow a comparison. In bubble flow, however, the few comparable data of this study and that of Guerrero are in agreement. This provides some support for the assertion that the total power determines the CHF in this regime. Even though the Guerrero data were determined by flooding of the

apparatus and not by actual flow diversion and overheating, these results may be directly compared.

In this study, downward flow with entrained air has been shown to exhibit distinctive characteristics according to the prevailing flow pattern. These are evident in unheated flow, in heated operation, and in the manner of overheating. The annular flow pattern is indicated by a two-region pressure profile and entrains little air. Fluid thermocouples are primarily in the gas phase and provide time-averaged readings above the equilibrium temperature, except in the liquid region at the bottom of the test section. CHF occurs when countercurrent flow limitation prevents cooling in the mid-region of the test section. The upward flowing vapor diverts the inlet flow to the bypass, and the whole test section overheats.

The intermittent pattern is dominated by axial mixing, driven by large bubbles. The rate of gas entrainment is high, and pressure, flow, and temperature signals fluctuate strongly. The presence of interacting parallel channels within the test section is hypothesized to allow a large bubble to stagnate and dry out the heater wall. This process has some random character to it, in that CHF often occurs only after some time has passed after increasing power. Furthermore, it has some arbitrary character, in that the power might be somewhat different if the temperature criterion were set to another value. The high wall temperatures are confined to a small part of a single subchannel. Overheating occurs significantly below saturated outlet conditions.

In the bubble flow pattern, the gas phase is broken into smaller dispersed units. Entrainment rate decreases, the flow behavior is more steady, and the time-averaged temperature profiles approach equilibrium. Overheating occurs in the channel at large, displacing the inlet flow to the bypass. The higher heat fluxes associated with the higher flow lead to rapid temperature rise and violent flow behavior. While the overheating occurs at subcooled outlet conditions, the efficiency of coolant usage is still greater than in the intermittent flow pattern. The approach to CHF resembles that of a single component Ledinegg instability.

In all the flow patterns, there is a need for improved mechanistic understanding. Although fairly plausible concepts have been advanced to explain the observed manner of overheating, there is no satisfactory means of quantitative prediction.

CONCLUSION

This study has examined the cooling of a heated vertical annular channel by gravity flow of water with entrainment of air. A bypass made the test section typical of a heated channel in gravity-fed, parallel array. The annulus was divided into subchannels by four longitudinal fins, and the heat flux varied around the periphery of the heater tube.

Visual examination of the air/water flow in a subdivided annulus indicates three main flow patterns. These - annular, intermittent, and bubble - have previously been observed in tube flow. In the present study, these patterns have exhibited distinct differences in their flow, heating, and overheating characteristics. Approximate conditions for their transition have been set.

Critical heat flux occurs at subcooled outlet conditions for all but the lowest flow rates. The azimuthal tilt causes one subchannel to run hot. This is most influential in the intermittent flow pattern, where the local heat flux seems to determine the rate of dryout under a stagnant bubble. The presence of fins, by providing partial segregation of the flow, probably exacerbates the dryout. In other flow patterns, it is rather the overall power which seems to be significant, in agreement with previous investigators.

Characteristics have been identified, and some discussion of mechanisms has been made, but further work is required to provide a complete description of the overheating behavior. While this paper has attempted to contrast the flow patterns, future experimentation may concentrate on the transition of one pattern into another.

ACKNOWLEDGMENTS

The equipment was designed by T. J. Steeper. D. A. Foreman, M. A. Lee, and E. W. Calk contributed to its construction and operation. The guidance of J. L. Steimke was most helpful, as were conversations with L. L. Hamm and G. P. Flach.

NOTATION

A_f flow area

A_h	heated area
C	empirical flooding coefficient
C_o	distribution coefficient characterizing radial profiles of void and velocity
C_p	liquid heat capacity
D_1	large dimension of rectangle
D_2	small dimension of rectangle
D_h	hydraulic diameter, or other appropriate characteristic length
g	acceleration due to gravity
G	mass velocity
h_{lg}	latent heat of vaporization
$<j>$	area-average total volumetric flux, $<j_g>$ + $<j_l>$
$<j_g>$	area-average gas volumetric flux, or superficial velocity
$<j_l>$	area-average liquid volumetric flux, or superficial velocity
P	pressure
Pe	Peclet number
T_b	bulk temperature of liquid at some axial position
T_i	inlet temperature of liquid
T_s	saturation temperature at prevailing pressure
U_t	terminal velocity of a large bubble in a rectangular channel
$<<V_{gj}>>$	weighted mean drift velocity
z	axial position
$<\alpha>$	area-average void fraction
ρ_g	gas phase density
ρ_l	liquid phase density
ϕ	heat flux

LITERATURE CITED

Barnea, D., Shoham, O., and Taitel, Y., 1982, "Flow Pattern Transition for Vertical Downward Two Phase Flow", Chemical Engineering Science, Vol. 37, No. 5, p. 741.

Block, J. A., and Wallis, G. B., 1978, "Heat Transfer and Fluid Flows Limited by Flooding", AIChE Symposium Series, Vol. 74, No. 174, p. 73.

Boure, J. A., Bergles, A. E., and Tong, L. S., 1973, "Review of Two-Phase Flow Instability", Nuclear Engineering and Design, Vol. 25, p. 165.

Butterworth, D. and Hewitt, G. F., 1977, Two-Phase Flow and Heat Transfer, Oxford University Press, Chapter 4.

Clark, N. N. and Flemmer, R. L. C., 1984, "On vertical downward two phase flow", Chemical Engineering Science, Vol. 39, No. 1, p. 170.

Clift, R., Grace, J. R., and Weber, M. E., 1978, Bubbles, Drops, and Particles, Academic Press, Chapter 9, Section III.

Crawford, T. J., Weinberger, C. B., and Weisman, J., 1985, "Two-Phase Flow Patterns and Void Fractions in Downward Flow. Part I: Steady-State Flow Patterns", International Journal of Multiphase Flow, Vol. 11, No. 6, p. 761.

Guerrero, H. N., 1990, "Emergency Cooling Simulation Tests on an Electrically Heated Channel Typical of SRP Reactor Fuel channels - Rig B", Proceedings Volume II, ANS International Topical Meeting, Boise, Idaho.

Golan, L. P., and Stenning, A. H., 1969, "Two-Phase Vertical Flow Maps", Proceedings of the Institution of Mechanical Engineers, Vol. 184, Pt. 3C, p. 108.

Kelessidis, V. C. and Dukler, A. E., 1989, "Modeling Flow Pattern Transitions for Upward Gas-Liquid Flow in Vertical Concentric and Eccentric Annuli", International Journal of Multiphase Flow, Vol. 15, No. 2, p. 173.

McQuillan, K. W. and Whalley, P. B., 1985, "Flow Patterns in Vertical Two-Phase Flow", International Journal of Multiphase Flow, Vol. 11, No. 2, p. 161.

Mishima, K. and Nishihara, H., 1985, "The Effect of Flow Direction and Magnitude on CHF for Low Pressure Water in Thin Rectangular Channels", Nuclear Engineering and Design, Vol. 86, p. 165.

Osakabe, M., and Kawasaki, Y., 1989, "Top Flooding in Thin Rectangular and Annular Passages", International Journal of Multiphase Flow, Vol. 15, No. 5, pp. 747-754.

Oshinowo, T., and Charles, M. E., 1974, "Vertical Two-Phase Flow. Part I. Flow Pattern Correlations", The Canadian Journal of Chemical Engineering, Vol. 52, p. 25.

Saha, P. and Zuber, N., 1974, "Point of Net Vapor Generation and Vapor Void Fraction in Subcooled Boiling", Proceedings of the Fifth International Heat Transfer Conference, Tokyo, p. 175.

Spedding, P. L., and Nguyen, V. T., 1980, "Regime maps for Air Water Two Phase Flow", Chemical Engineering Science, Vol. 35, p. 779.

Sudo, Y., Miyata, K., Ikawa, H., Kaminaga, M., and Ohkawara, M., 1985, "Experimental Study of Differences in DNB Heat Flux between Upflow and Downflow in Vertical Rectangular Channel", Journal of Nuclear Science and Technology, Vol. 22, No. 8, p. 604.

Wallis, G. B., 1969, One-Dimensional Two-Phase Flow, McGraw-Hill, Chapter 11.

Yamazaki, Y., and Yamaguchi, K., 1979, "Characteristics of Cocurrent Two-Phase Downflow in Tubes", Journal of Nuclear Science and Technology, Vol. 16, No. 4, p. 245.

Zuber, N. and Findlay, J. A., 1965, "Average Volumetric Concentration in Two-Phase Flow Systems, Trans. ASME, Journal of Heat Transfer, Vol. 87, p. 453.

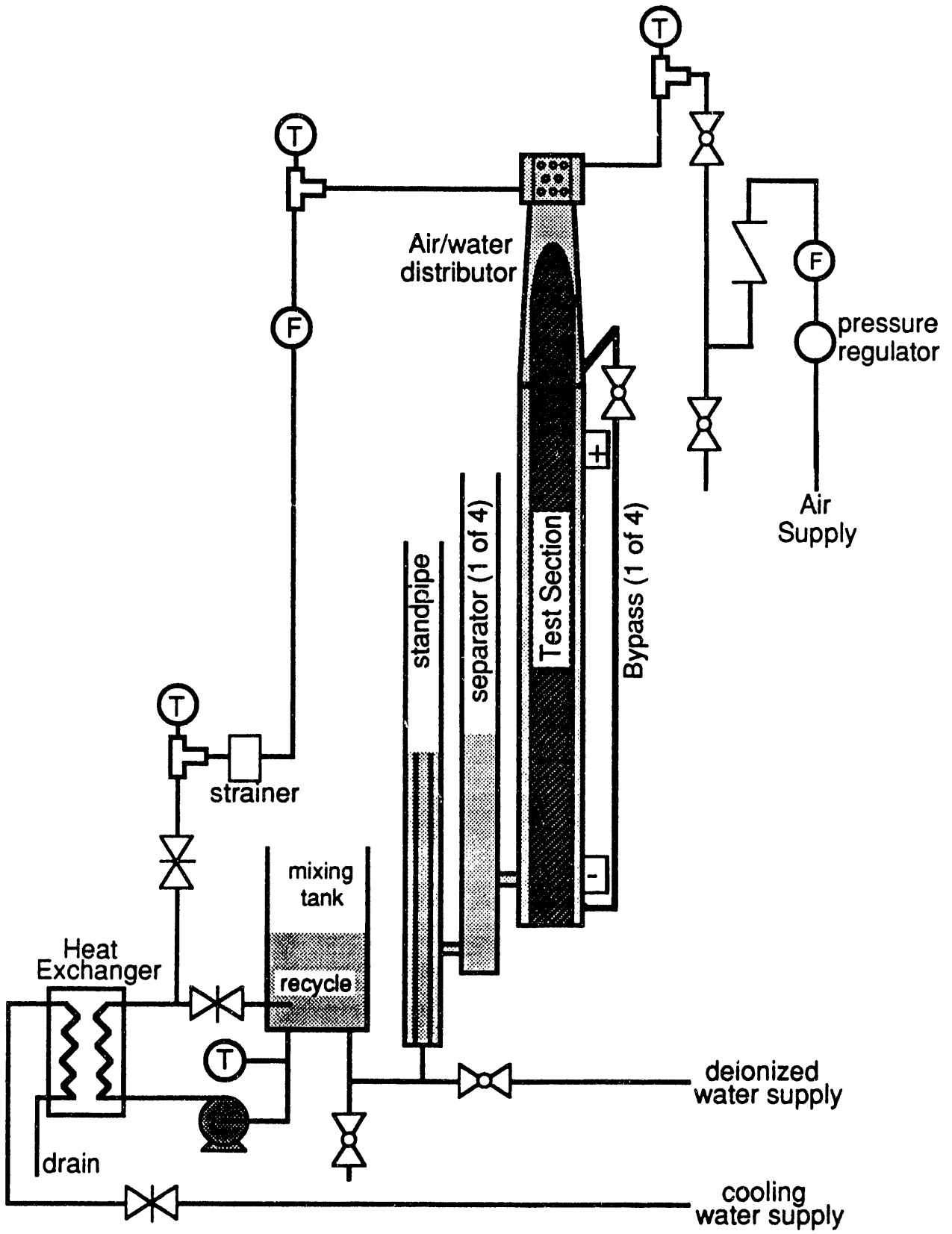

Figure 1. Schematic of Test Loop

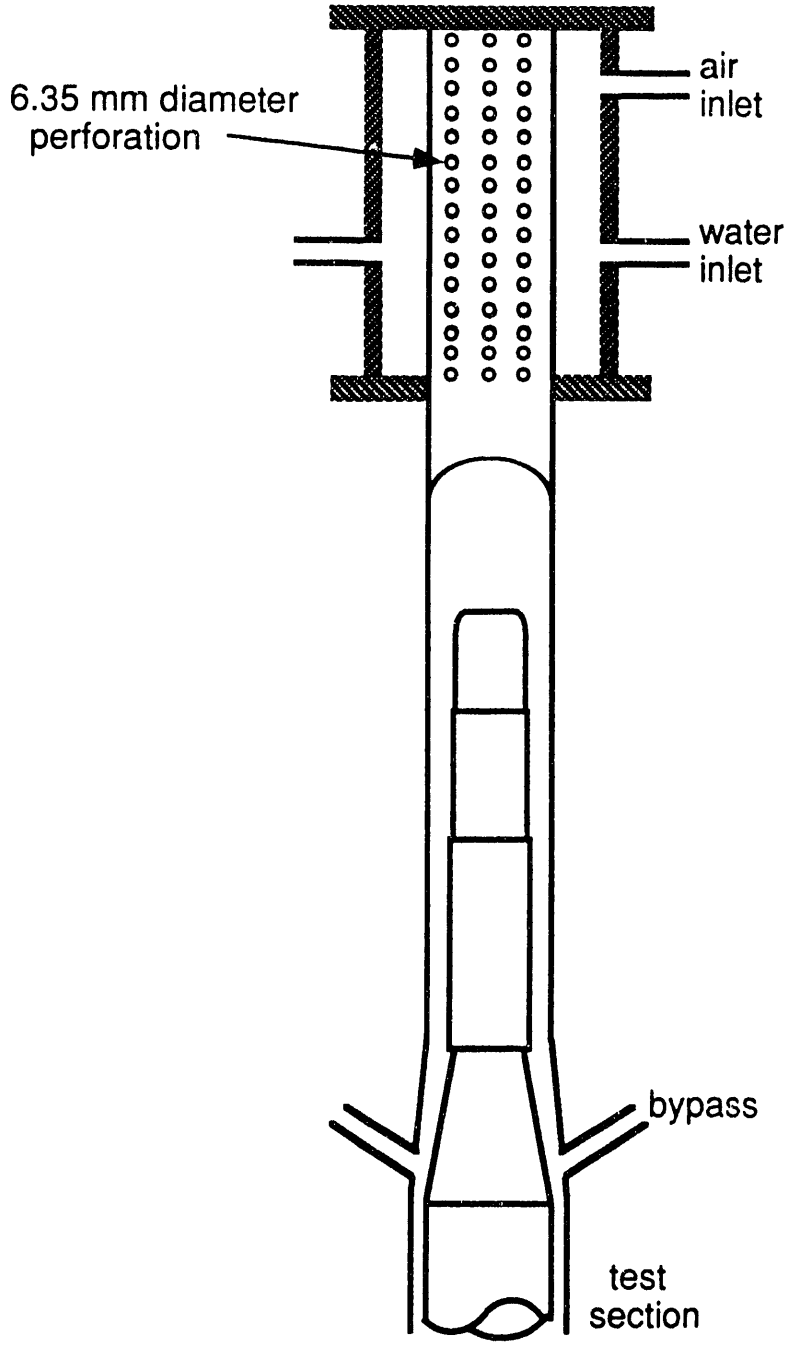

Figure 2. Air/water Distributor

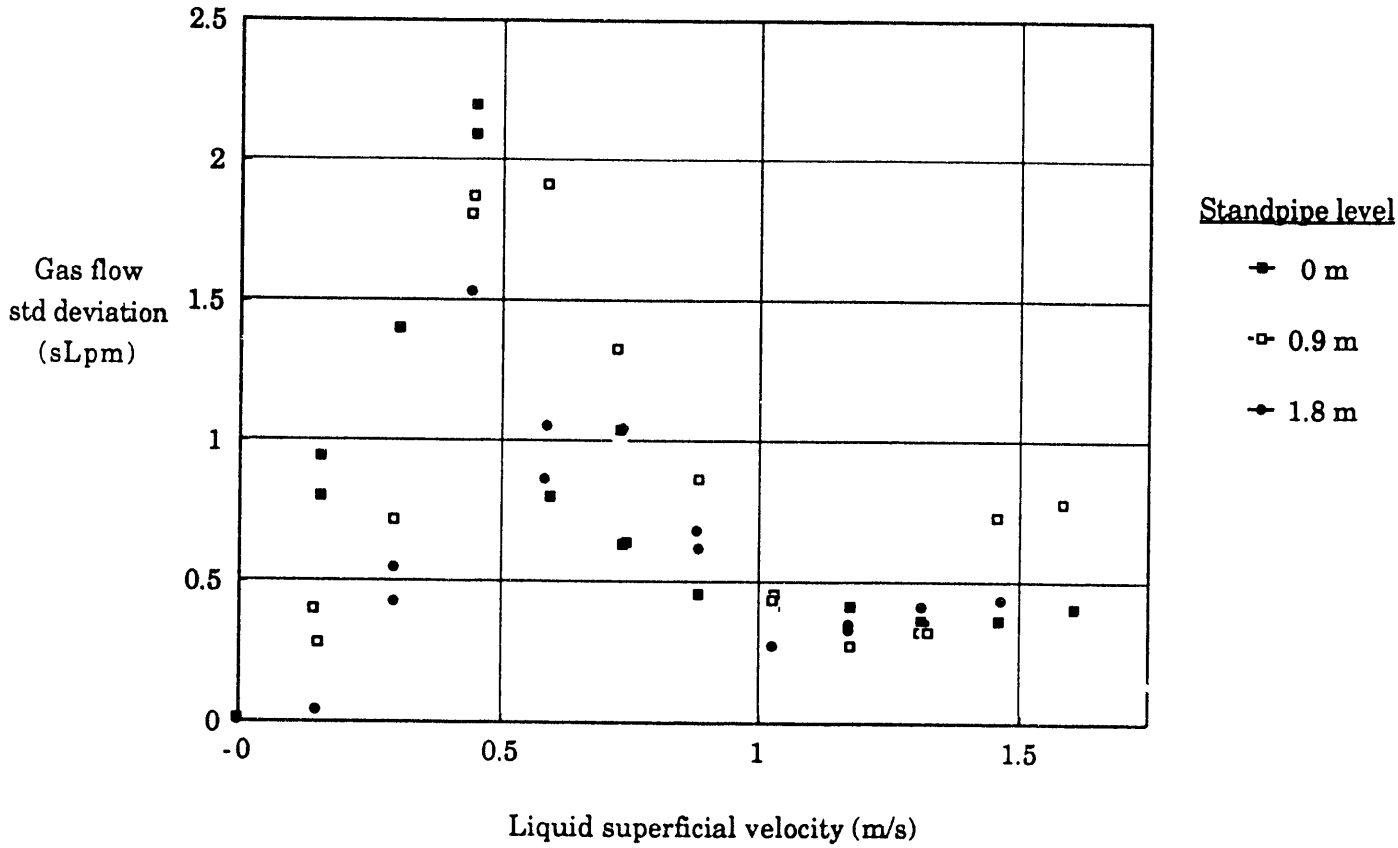

Figure 4. **Fluctuations in entrained air flow rate as a function of imposed liquid flow for three different standpipe levels.**

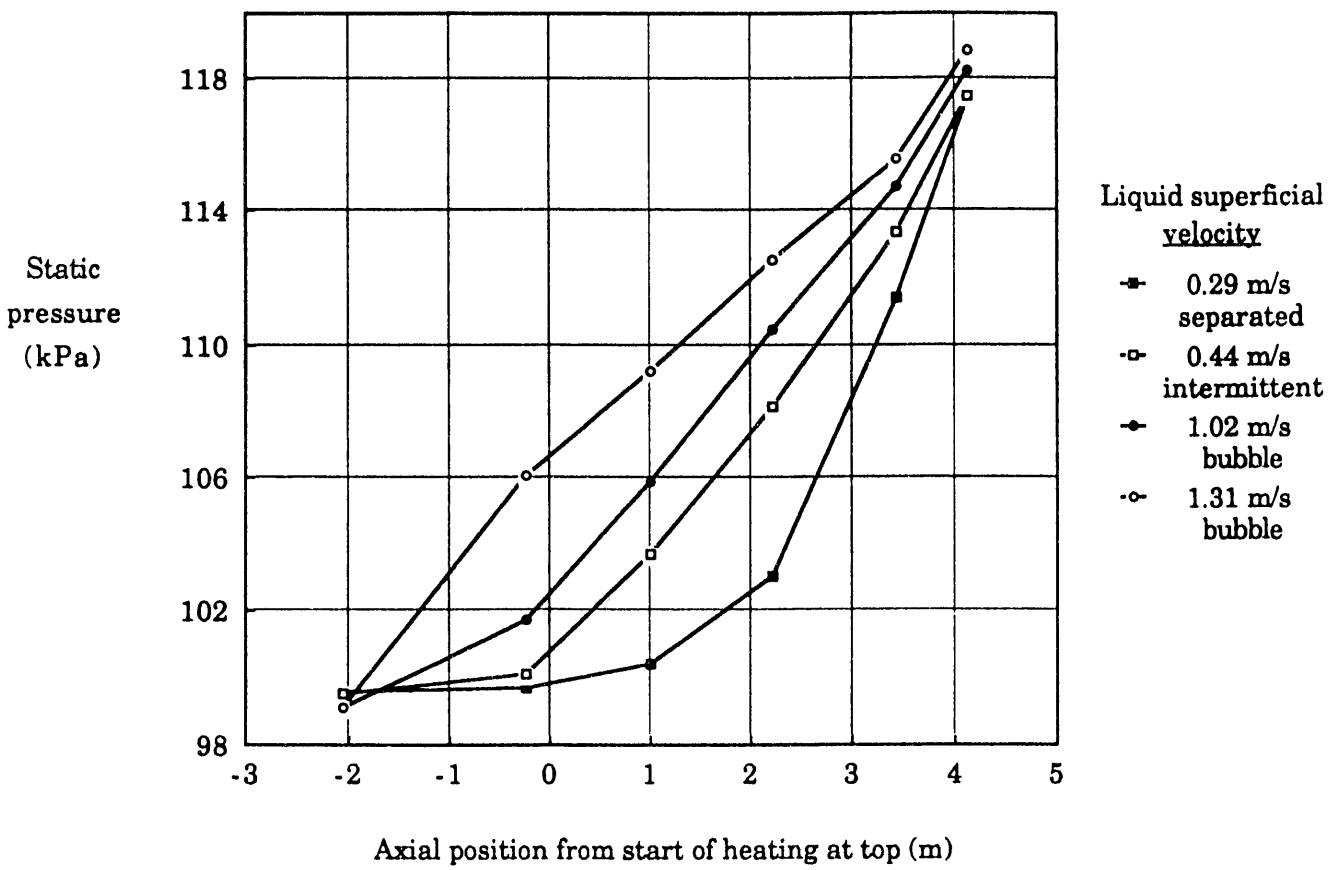

Figure 5. Pressure distribution at various imposed liquid flows for a standpipe level of 1.8 m. The inner four points in each profile are in the test section itself.

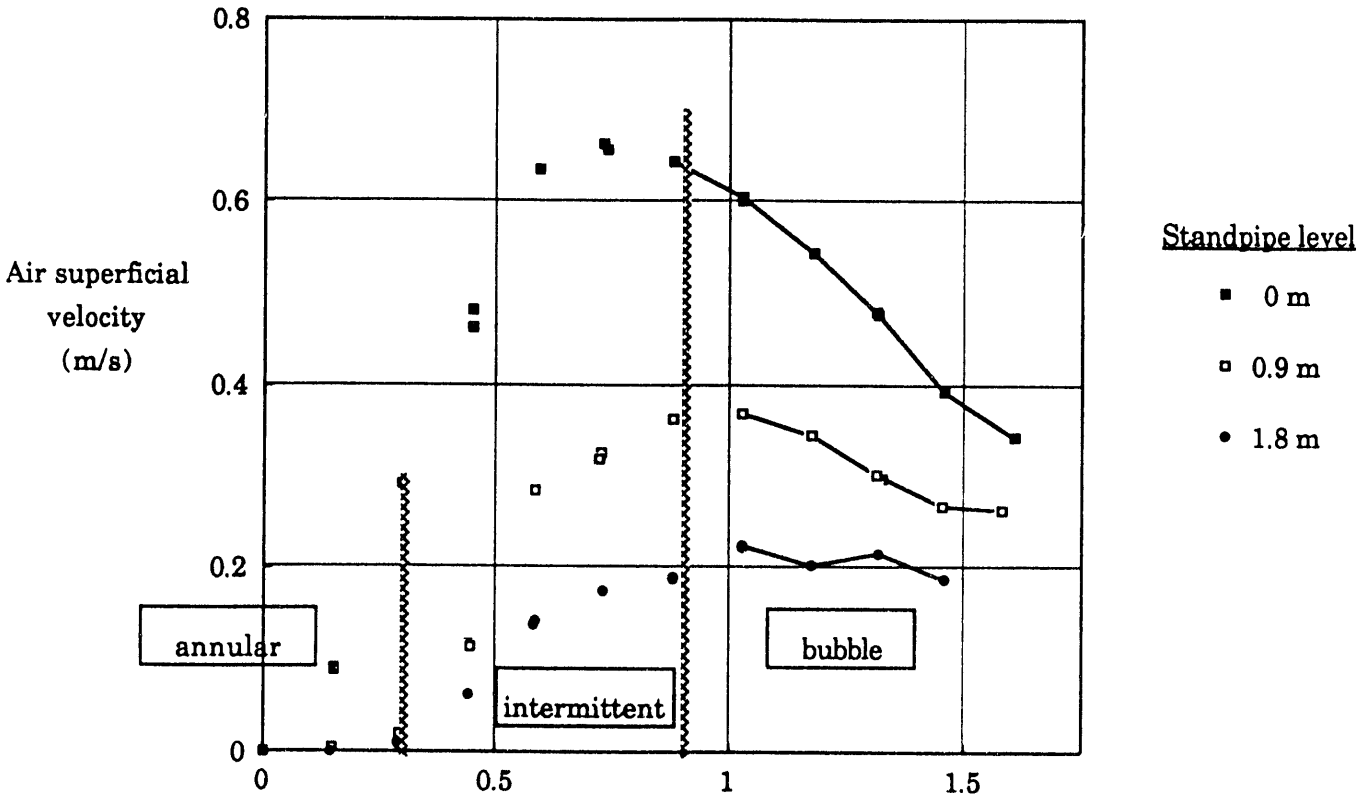

Figure 6. Air entrained by imposed liquid flow for three different liquid levels in exit standpipe. The connected points are those from the asymptotic region in Figure 3.

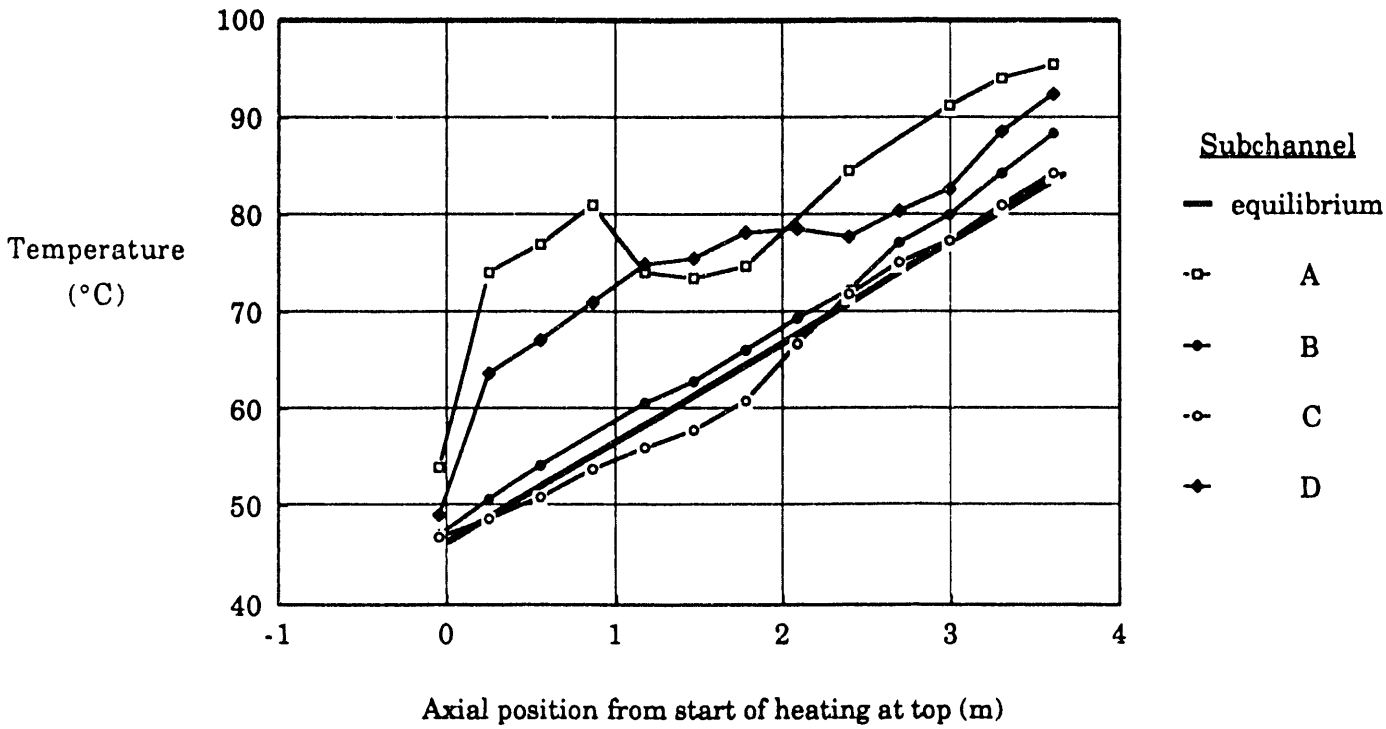

Figure 7. Axial distribution of time-averaged fluid temperature in each subchannel. Liquid superficial velocity 0.59 m/s, intermittent flow pattern, average heat flux 91.9 kW/m2, outlet saturation temperature 101.9°C.

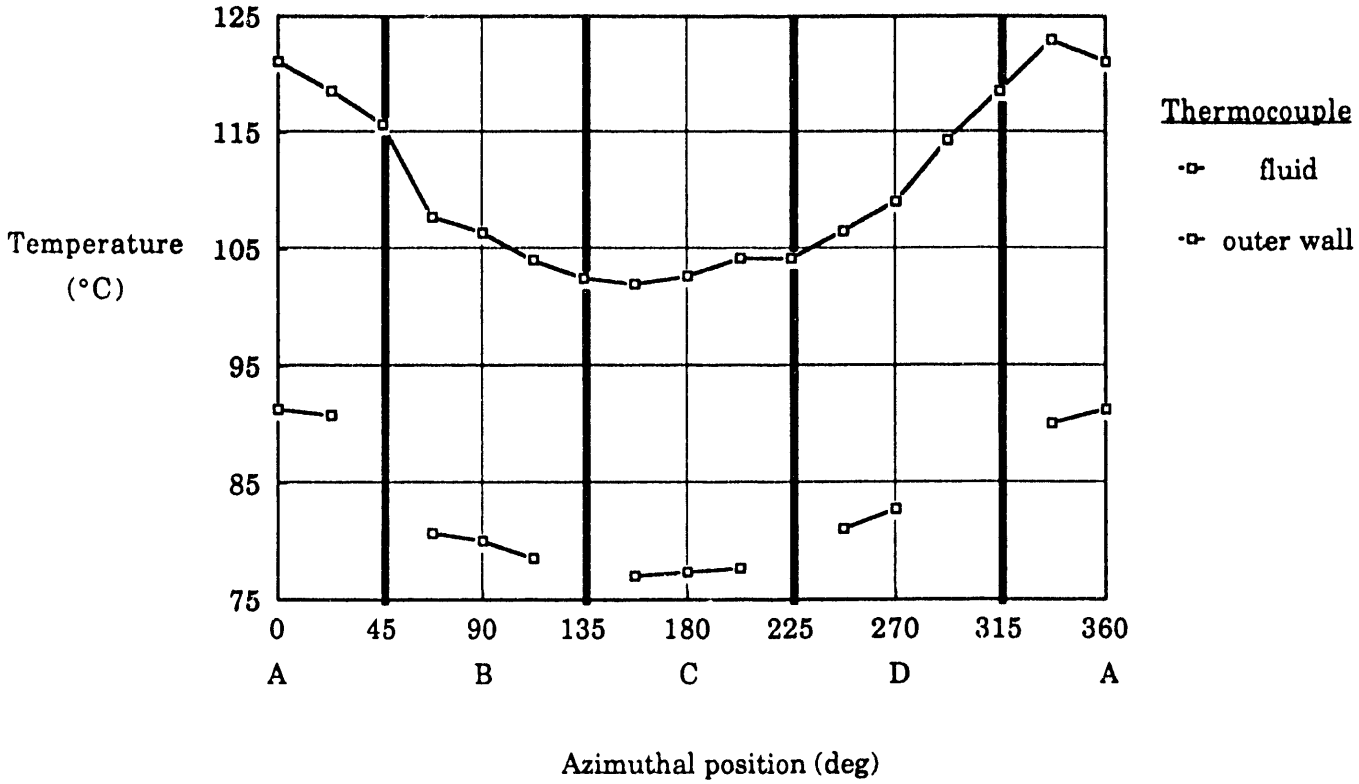

Figure 8. Azimuthal distribution of time-averaged wall and fluid temperature at one axial position. Fins at 45°, 135°, 225°, and 315°. Liquid superficial velocity 0.59 m/s, intermittent flow pattern, average heat flux 91.9 kW/m2, outlet saturation temperature 101.9°C.

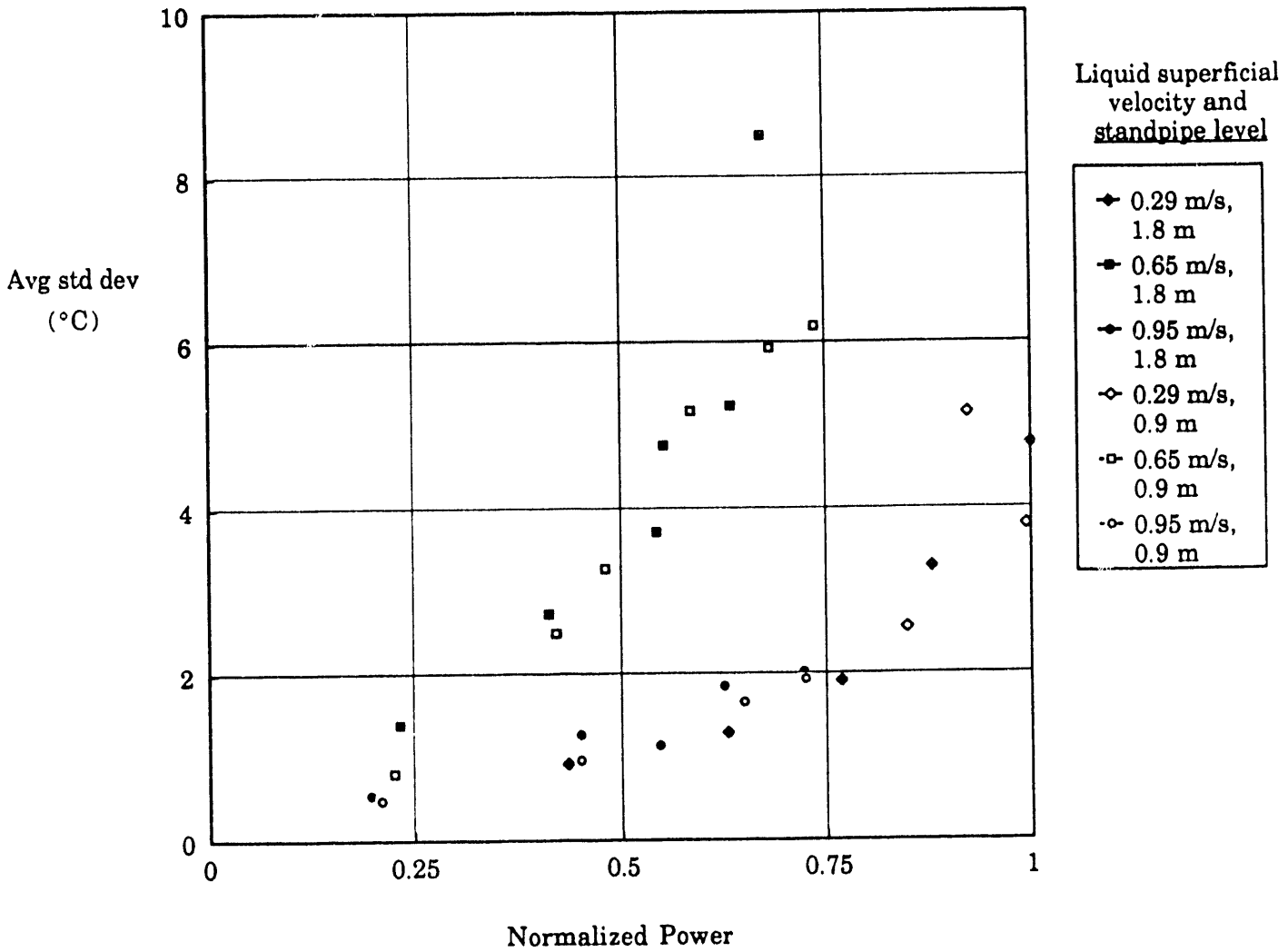

Figure 9. Fluctuation in fluid temperature, indicated by the average of the standard deviations of individual traces, versus normalized power. Data are given for two standpipe levels and three superficial velocities.

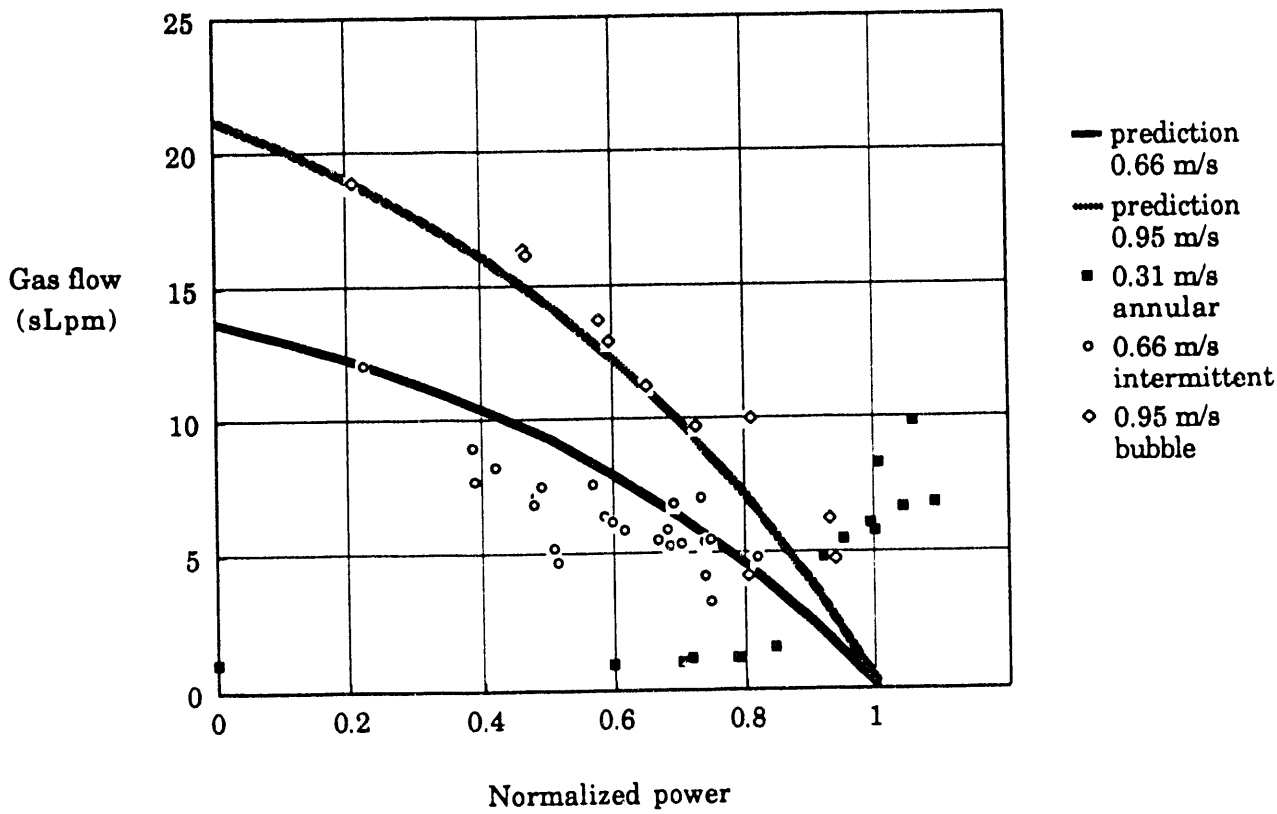

Figure 10. Variation in air entrainment with increasing power for three different liquid flows. Power is normalized by power required for saturated outlet temperature.

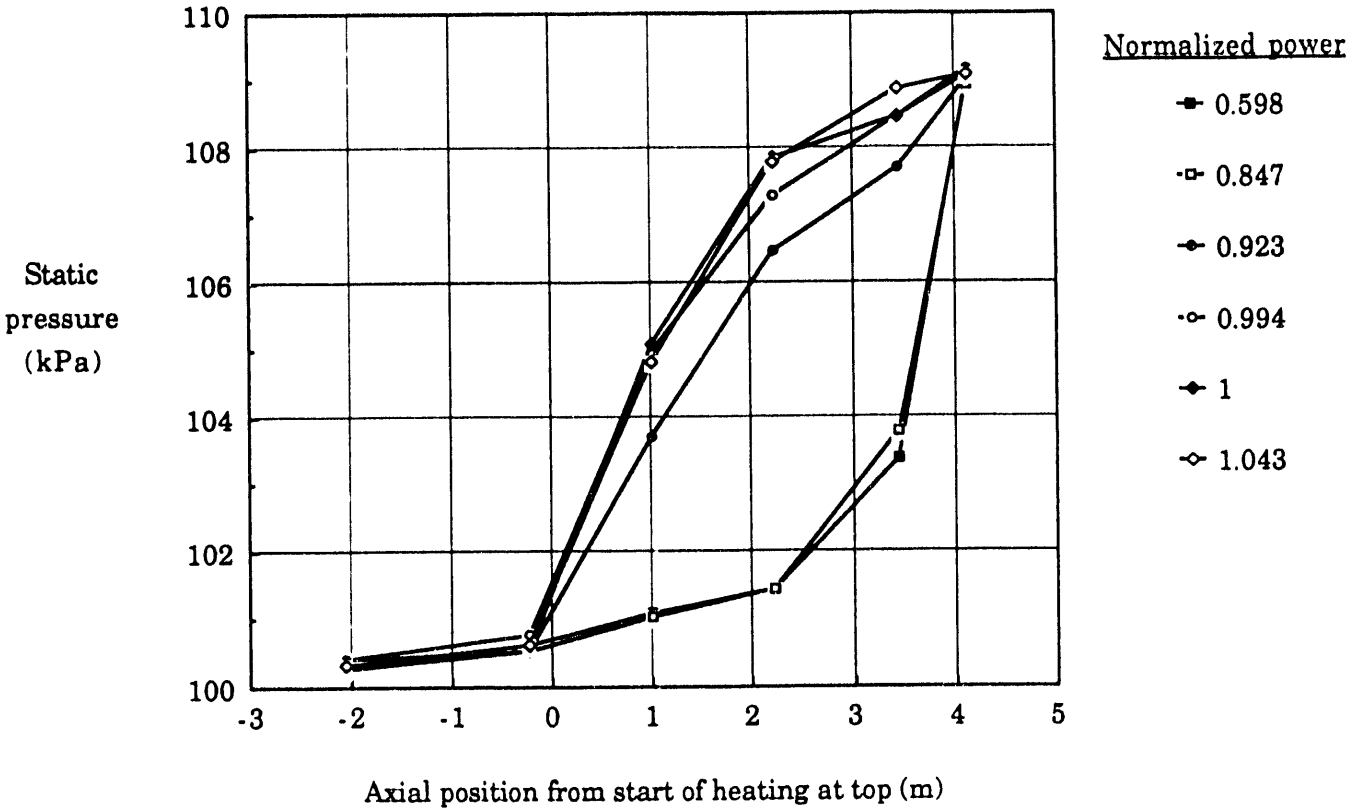

Figure 11. Change in axial pressure profile for annular flow pattern as power is increased. Power is normalized by power required for saturated outlet temperature. Liquid superficial velocity 0.31 m/s, 0.9 m standpipe liquid level.

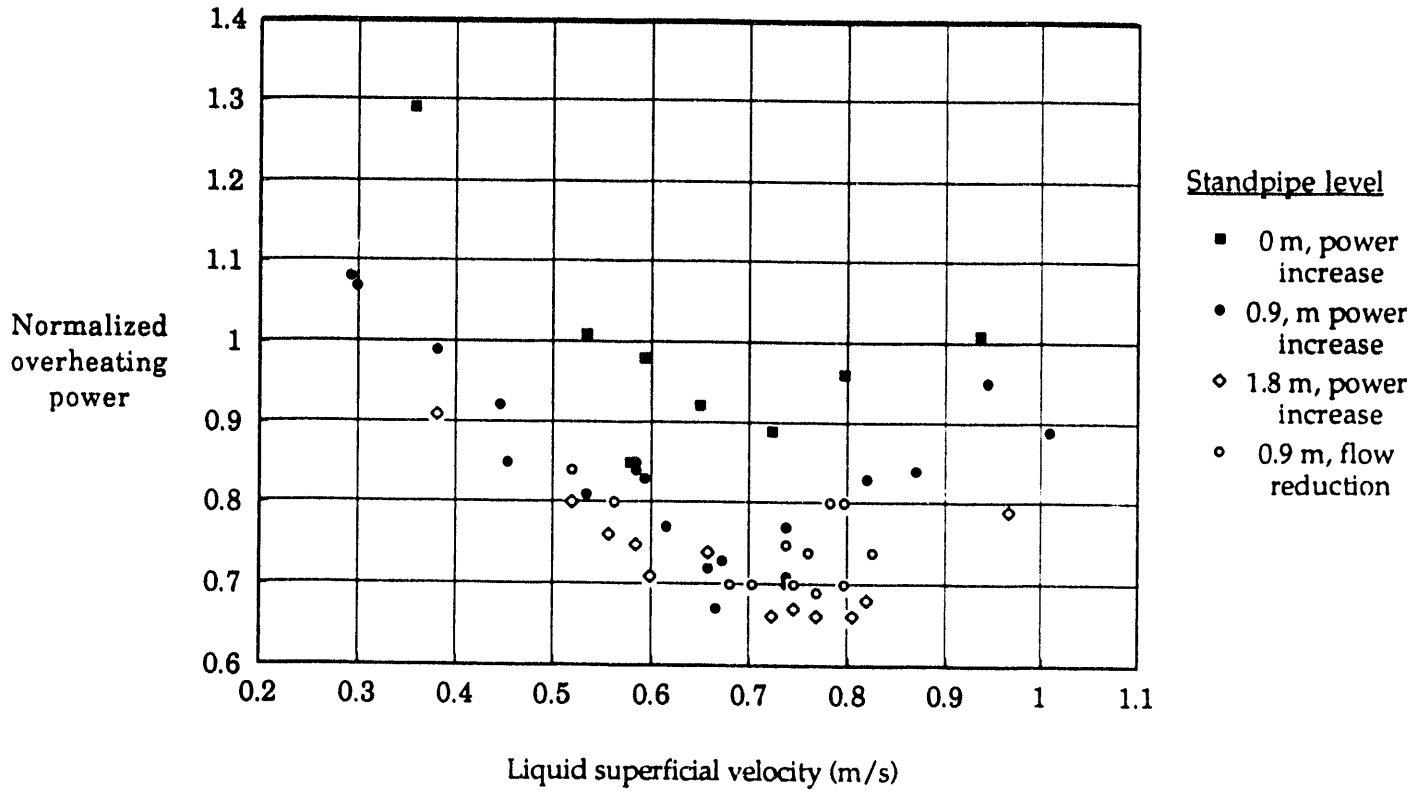

Figure 12. Normalized power for overheating as a function of imposed liquid flow for three different standpipe liquid levels.

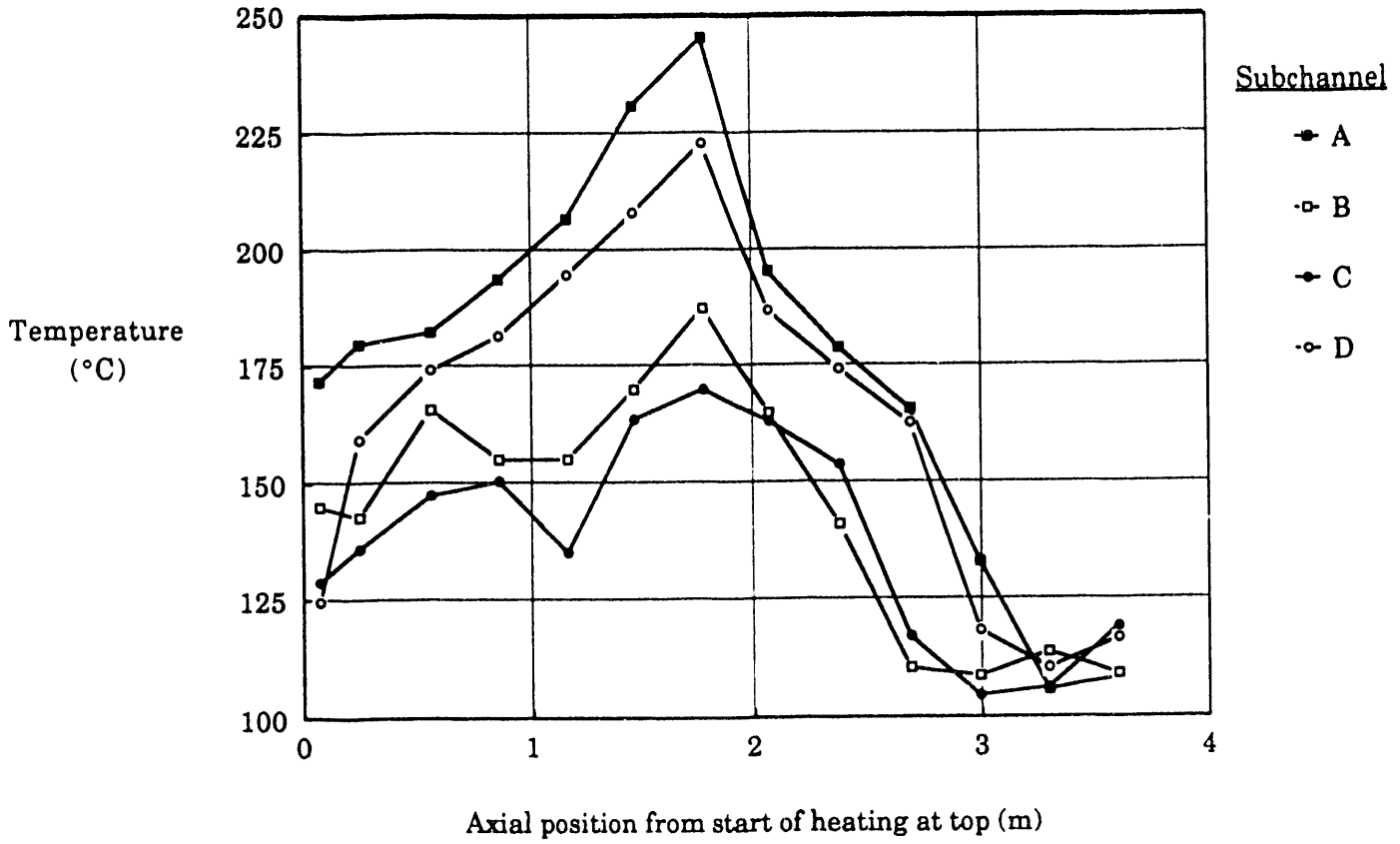

Figure 13. Axial temperature profiles averaged over five-second interval at power scram. Liquid superficial velocity 0.31 m/s, average heat flux 80.0 kW/m2, outlet saturation temperature 102.1°C.

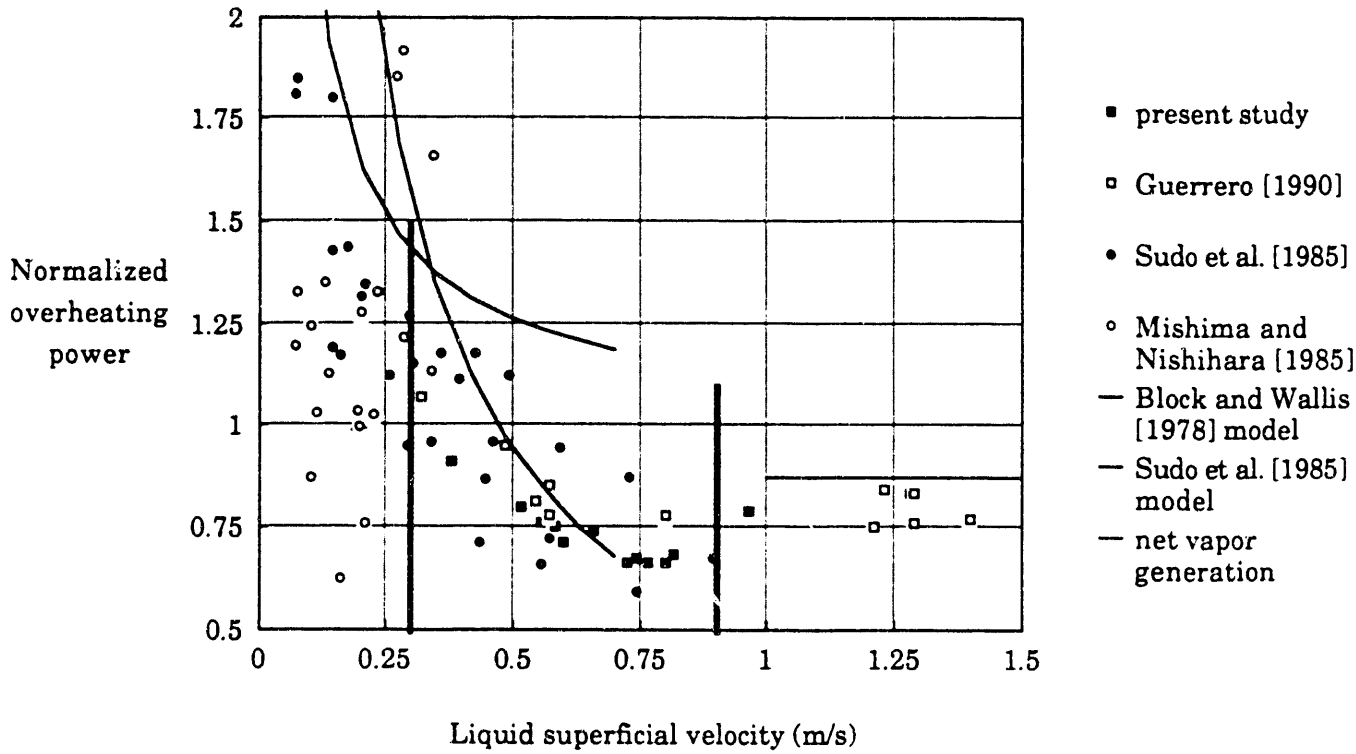

Figure 14. Normalized power for overheating as a function of imposed liquid flow, including data from the present study and others, with models based on flooding and net vapor generation.

END

DATE
FILMED
12/7/92